

Valence-difference contrast measurements utilizing X-ray anomalous scattering

Satoshi Sasaki,* Takeshi Toyoda, Kouji Yamawaki and Koichi Ohkubo

Materials and Structures Laboratory, Tokyo Institute of Technology, Nagatsuta 4259, Midori, Yokohama 226-8503, Japan. E-mail: sasaki@n.cc.titech.ac.jp

(Received 4 August 1997; accepted 27 November 1997)

Anomalous scattering experiments with X-ray wavelengths close to an absorption edge have made it possible to determine independently the behaviour of ions in different valence states. The anomalous scattering factors of Fe^{2+} and Fe^{3+} obtained from both absorption and diffraction data have a large difference in f' between the two kinds of ions. Using a valence-difference contrast method, Bragg and diffuse scattering measurements were carried out for single crystals of Fe_3O_4 at low temperatures. The results demonstrate the ability of the contrast method to resolve charge ordering and valence fluctuation details.

Keywords: valence-difference contrast methods; valence contrast methods; anomalous scattering; magnetite; Fe_3O_4 .

1. Introduction

X-ray diffraction is a powerful tool to determine a crystal structure composed of several kinds of atoms, where the determination ability depends upon the difference in atomic scattering factors. The difference can be enhanced when the anomalous scattering effect is dominant at a wavelength close to an absorption edge. In XANES (X-ray absorption near-edge structure) spectra, it is known that the change of the energy levels of valence electrons

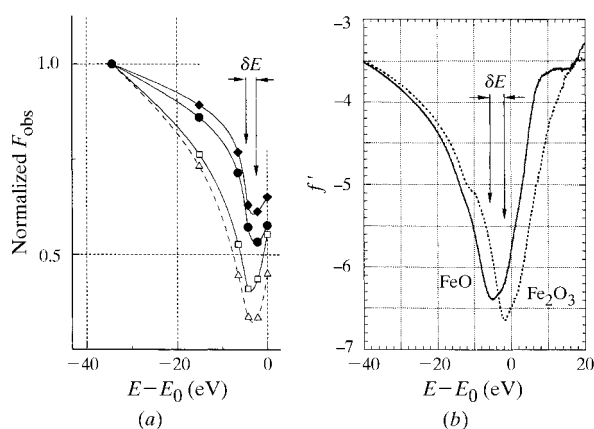


Figure 1

Energy dependency of the diffraction intensity and f' versus chemical shift δE . (a) The crystal structure factors are normalized at $\lambda = 1.7499$ Å ($E - E_0 = -34.3$ eV), where E_0 is at a second inflection point of the absorption curve of FeO. The 222 (open squares) and 226 (open triangles) reflections are mainly affected by the Fe^{2+} and Fe^{3+} of the B sites, while the 224 (solid squares) and the 026 (solid circles) reflections are contributed to only by the Fe^{3+} of the A sites. (b) Experimental f' values for Fe^{2+} (solid line; FeO) and Fe^{3+} (dashed line; Fe_2O_3) obtained by the Kramers–Kronig transform of the XANES spectra.

gives a chemical shift of up to several eV. The oxidation numbers for various valence ions cause chemical shifts on pre- and main-edge peaks (Sarode *et al.*, 1979). The use of anomalous scattering for different oxidation states is a relatively new technique, although many attempts have been made, for example, for such compounds as Eu_3O_4 , $\alpha\text{-Fe}_2\text{PO}_5$, Fe_3O_4 , $\text{YBa}_2\text{Cu}_3\text{O}_6$, GaCl_2 and NbSe_3 (Kwei *et al.*, 1990; Atfield, 1990; Wilkinson *et al.*, 1991; Warner *et al.*, 1992; Gao *et al.*, 1992, 1993; Sasaki, 1995; Toyoda *et al.*, 1997). It is still in dispute whether such f' values have enough accuracy to be of practical use in structural refinements.

In the coordination of octahedral O atoms, a chemical shift between Fe^{2+} and Fe^{3+} ions has been estimated as 5 eV from the observation of XANES spectra (Sasaki, 1995). Based on the algorithm by Cromer & Liberman (1970) and absorption data, experimental f' values have been reported for Fe^{2+} and Fe^{3+} ions, where there is a large f' difference of 2.5 between ferrous and ferric ions at $\lambda = 1.7415$ Å. The Kramers–Kronig transformation is also useful to estimate f' from f'' .

In this paper we aim to establish a method to contrast valence differences. We examine experimental f' values for making the contrast, based on the wavelength-dependent diffraction intensities of Fe_3O_4 at the Fe K-edge. Furthermore, we demonstrate the ability of the valence-difference contrast method to determine charge ordering and valence fluctuation at low temperatures.

2. Experimental

Magnetite (Fe_3O_4 , inverse-spinel structure, cubic, $Fd\bar{3}m$, $a = 8.375 \pm 0.002$ Å) was used in this study. The single crystals were prepared by several methods: (S1) a spherical crystal, 0.08 mm in diameter, grown from Fe_3O_4 powders at 1300 K in an evacuated silica tube; (S2) a spherical crystal, 0.13 mm in diameter, grown from Fe_3O_4 powders at 673 K in a 5M NH_4Cl solution in an Au tube; (S3) a parallelepiped crystal of $0.3 \times 0.3 \times 0.3$ mm grown from Fe_3O_4 powders in a Pt–10%Rh crucible by the Bridgman method in a CO–CO₂ atmosphere. Spherical crystals were prepared by air-rolling on fine sandpaper by the Bond method.

Synchrotron experiments were performed at BL-10A at the Photon Factory using a vertical-type four-circle diffractometer. An Si(111) monochromator was used in a horizontal dispersion setting to select the X-ray wavelengths. Wavelength calibrations were made by measuring the XANES spectra of Fe foil and FeO.

3. Wavelength dependency of anomalous scattering factors

Magnetite has two kinds of crystallographically distinguished cation sites, A and B, where the tetrahedral A site is occupied only by Fe^{3+} ions and the octahedral B site is equally occupied by Fe^{2+} and Fe^{3+} ions. From the occupancy difference of Fe ions between the two sites, a feasibility study on f' values has been carried out.

Intensity profiles of magnetite (S1) were collected in ω – 2θ step-scan mode for seven wavelengths at the longer wavelength side of the Fe K-absorption edge: $\lambda = 1.7415, 1.7420, 1.7425, 1.7431, 1.7452, 1.7499$ and 1.7567 Å, corresponding to 0, –2.2, –4.3, –6.5, –15.1, –34.3 and –61.9 eV in $E - E_0$, respectively. Each profile consists of 80 steps at an ω interval of 0.02° measured for 1 s per step. The intensity decrease of the incident beam was corrected using the 222 reflection as a standard. Each set of integrated intensities was corrected for the Lorentz polarization factor and the absorption effect.

The wavelength dependency of the observed structure factors, F_{obs} , is plotted in Fig. 1(a). A chemical shift, δE , can be observed

between the *A* and *B* sites which corresponds to a valence difference of 0.5 e. It is noted that the normalized F_{obs} related to the *B* sites is smaller than that of the *A* sites, and is comparable with the change of f' in Fig. 1(b). It implies that the *A* sites are mostly occupied by Fe^{3+} , while the *B* sites can be assigned to $\text{Fe}^{2.5+}$ as a result of the continuous interchange of electrons between Fe^{2+} and Fe^{3+} . Thus, the existence of the f' difference between the two sites is indeed promising for studying mixed-valence compounds.

4. Low-temperature crystallography

The high electrical conductivity of magnetite at room temperature appears to be due to ‘hopping’ in a mixed-valence state between Fe^{2+} and Fe^{3+} . The spinel phase transforms to a lower symmetry form below the Verwey transition temperature ($T_V \simeq 123$ K). Verwey *et al.* (1947) proposed an ordering scheme in which alternative Fe^{2+} and Fe^{3+} ions exist along the *c* axis. Samuelsen *et al.* (1968) and Yamada *et al.* (1968) reported observations of the $(h, 0, l + \frac{1}{2})$ -type reflections by neutron and electron diffraction methods, respectively. Several authors proposed the structure of a low-temperature phase based on a rhombohedral, monoclinic or triclinic cell (*e.g.* Iizumi *et al.*, 1982). However, complicated twinning below T_V still remains a controversy for this crystal structure.

Low-temperature experiments were conducted at 102 K using a cooling device to generate a cold and dry gas stream from liquid nitrogen, blown directly onto the crystal (S2). The temperature calibration was made at the sample position (Toyoda *et al.*, 1997). Intensity data were collected using the ω - 2θ step-scan mode within a hemisphere (or one-eighth) of reciprocal space up to $2\theta = 114^\circ$.

Fig. 2 shows the intensity profiles of extra reflections indexed as (a) $0\ 3\frac{1}{2}\ 4$ and $0\ 4\frac{1}{2}\ 4$, and (b) $0\ 4\ 3\frac{1}{2}$ and $0\ 4\ 4\frac{1}{2}$, based on a cubic cell, suggesting the existence of a low-temperature phase of magnetite. A subset of the half-indexed reflections are listed in Table 1. The extra reflections are caused by a lowering of the crystal symmetry where there would be charge ordering of Fe^{2+} and Fe^{3+} ions as well as the lattice deformation associated with atomic position shifts. The space group obtained here is *Cmcm* with a doubled cell of $\mathbf{a} = 2\mathbf{a}_1 + 2\mathbf{a}_2$, $\mathbf{b} = -2\mathbf{a}_1 + 2\mathbf{a}_2$, $\mathbf{c} = 2\mathbf{a}_3$. It is notable that in Fig. 2 the half-integer reflections give a large difference in diffraction

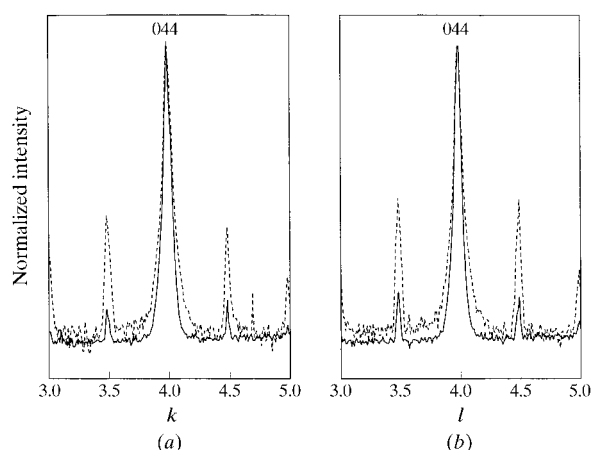


Figure 2

Variation of the logarithmic intensity versus the momentum transfer. The extra half-index reflections appear near 044 at $T = 102$ K and $\lambda = 1.7421$ Å (solid line) and 1.7499 Å (dashed line); (a) along the b^* axis, (b) along the c^* axis.

Table 1

Typical reflections having half-integer Miller indices hkl based on the cubic spinel cell.

hkl is related to $h'k'l'$ of an orthorhombic cell with a transform matrix, $(02\bar{2}022/200)$.

h	k	l	h'	k'	l'	F_{obs}
$4\frac{1}{2}$	4	0	8	8	9	15.10
0	$\frac{1}{2}$	4	-7	9	0	17.66
0	$4\frac{1}{2}$	4	1	17	0	21.49
0	$\frac{1}{2}$	$\frac{1}{2}$	0	2	0	15.65
0	4	$\frac{1}{2}$	7	9	0	15.52
0	4	$3\frac{1}{2}$	1	15	0	30.27
0	4	$4\frac{1}{2}$	-1	17	0	28.55
$\frac{1}{2}$	4	4	0	16	1	15.59
4	$\frac{1}{2}$	4	-7	9	8	20.67
$3\frac{1}{2}$	4	4	0	16	7	17.29
4	$3\frac{1}{2}$	4	-1	15	8	21.26
4	$4\frac{1}{2}$	4	1	17	8	17.06
4	4	$3\frac{1}{2}$	1	15	8	12.92
$3\frac{1}{2}$	0	4	-8	8	7	16.67

intensity between two wavelengths: $f'(\text{Fe}^{2+}) - f'(\text{Fe}^{3+}) = -1.6$ at $\lambda = 1.7421$ Å and -0.18 at $\lambda = 1.7499$ Å.

5. X-ray diffuse scattering

Diffuse scattering associated with charge ordering was studied using the valence-difference contrast method. A valence fluctua-

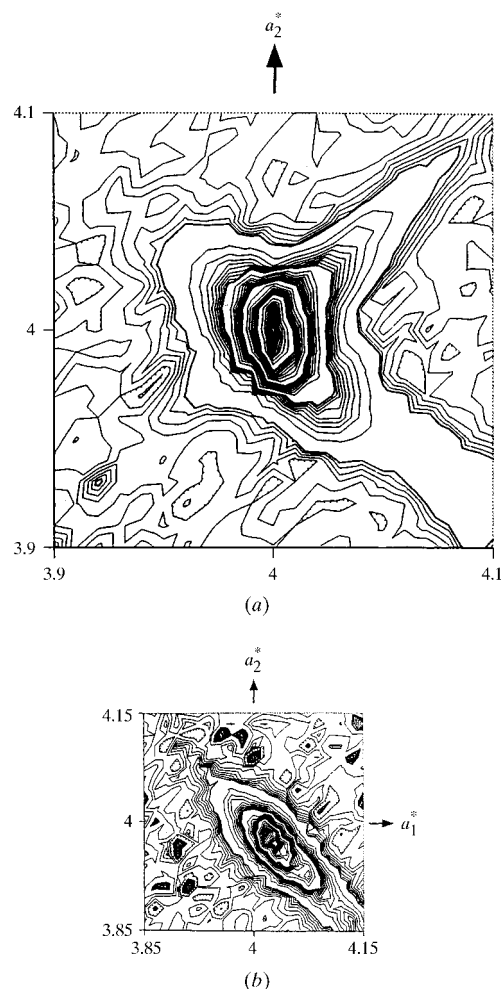


Figure 3

Observed intensity distribution of the X-ray diffuse scattering around 440: (a) $f'(\text{Fe}^{2+}) - f'(\text{Fe}^{3+}) = -1.60$, $\Delta E/E \simeq 10^{-4}$ and (b) $\Delta E/E \simeq 10^{-3}$. For both (a) and (b), $T = 130$ K and $\lambda = 1.7421$ Å.

tion between Fe^{2+} and Fe^{3+} ions above T_V was detected for the first time by means of X-ray scattering (Toyoda *et al.*, 1997). The appearance of similar diffuse streaks is already reported from neutron and electron diffraction studies, based on the contrast caused by the displacement of the O atoms (Shapiro *et al.*, 1976; Chiba *et al.*, 1975). A molecular polaron model has been proposed for the neutron diffuse streaks (Yamada *et al.*, 1979).

The wavelength used here is 1.7421 Å with an energy resolution of $\Delta E/E \simeq 10^{-4}$ and an f' difference of 1.6 between Fe^{2+} and Fe^{3+} . The 400, 800, 440, 221 and 444 reflections of magnetite (S3) were measured at 130 K by stationary counting of 10 s per step at each point of a 20×20 grid in the reciprocal lattice plane.

The intensity distribution of diffuse scattering around a 440 reciprocal lattice point is shown in an iso-diffusion surface (Fig. 3). The diffuse streaks shown in Fig. 3(a) elongate along the $[1\bar{1}0]^*$ direction characteristically. The elongating direction of the X-ray diffuse streaks significantly differs from that in neutron measurements. The X-ray diffuse distribution can be explained as a result of local charge ordering between Fe^{2+} and Fe^{3+} . A Huang scattering analysis was applied to determine the double-force tensor which produces partial ordering of Fe^{2+} and Fe^{3+} and the local displacement with the pairing ions among the B sites. The horn-like streaks disappeared with X-rays having a lower energy resolution (Fig. 3b, $\Delta E/E \simeq 10^{-3}$), where the energy width is larger than the energy shift between Fe^{2+} and Fe^{3+} . The diffuse scattering around $[110]^*$ is due to thermal diffuse scattering. Thus, the appearance of valence fluctuation assures the validity of the valence-difference contrast method.

We thank Drs H. Kawata, S. Todo and K. Tsukimura for magnetite crystals. This study was performed under the auspices

of the Photon Factory (PAC No. 95 G293) and supported by a Grant-in-Aid (07805001) and JSPS-RFTF96P00205.

References

- Attfield, J. P. (1990). *Nature (London)*, **343**, 46–49.
- Chiba, K., Suzuki, K. & Chikazumi, S. (1975). *J. Phys. Soc. Jpn*, **39**, 839–840.
- Cromer, D. T. & Liberman, D. (1970). *J. Chem. Phys.* **53**, 1891–1898.
- Gao, Y., Frost-Jensen, A., Pressprich, M. R. & Coppens, P. (1992). *J. Am. Chem. Soc.* **114**, 9214–9215.
- Gao, Y., Pressprich, M. R. & Coppens, P. (1993). *Acta Cryst.* **A49**, 216–219.
- Iizumi, M., Koetzle, T. F., Shirane, G., Chikazumi, S., Matsui, M. & Todo, S. (1982). *Acta Cryst.* **B38**, 2121–2133.
- Kwei, G. H., Dreele, R. B., Williams, A., Goldstone, J. A., Lawson A. C. & Warburton, W. K. (1990). *J. Mol. Struct.* **223**, 383–406.
- Samuelsen, J., Bleeker, E. J., Dobrzynski, L. & Riste, T. (1968). *J. Appl. Phys.* **39**, 1114–1115.
- Sarode, P. R., Ramasesha, S., Madhusudan, W. H. & Rao, C. N. R. (1979). *J. Phys. C*, **12**, 2439–2445.
- Sasaki, S. (1995). *Rev. Sci. Instrum.* **66**, 1573–1576.
- Shapiro, S. M., Iizumi, M. & Shirane, G. (1976). *Phys. Rev. B*, **14**, 200–207.
- Toyoda, T., Sasaki, S. & Tanaka, M. (1997). *Jpn. J. Appl. Phys.* **36**, 2247–2252.
- Verwey, E. J. W., Haayman, P. W. & Romeijn, F. C. (1947). *J. Chem. Phys.* **15**, 181–187.
- Warner, J. K., Cheetham, A. K., Cox, D. E. & Von Dreele, R. B. (1992). *J. Am. Chem. Soc.* **114**, 6074–6080.
- Wilkinson, A. P., Cheetham, A. K. & Cox, D. E. (1991). *Acta Cryst.* **B47**, 155–161.
- Yamada, T., Suzuki, K. & Chikazumi, S. (1968). *Appl. Phys. Lett.* **13**, 172–174.
- Yamada, Y., Mori, M., Noda, Y. & Iizumi, M. (1979). *Solid State Commun.* **32**, 827–830.